



Crystalline orientation effects on material removal of sapphire by femtosecond laser irradiation

Qiuling Wen^{a,*}, Pengcheng Zhang^a, Guanghua Cheng^b, Feng Jiang^a, Xizhao Lu^c

^a Institute of Manufacturing Engineering, Huaqiao University, Xiamen, 361021, Fujian, China

^b School of Electronics, Northwestern Polytechnical University, Xi'an, 710072, Shaanxi, China

^c College of Mechanical Engineering and Automation, Huaqiao University, Xiamen, 361021, Fujian, China

ARTICLE INFO

Keywords:

Femtosecond laser ablation
Sapphire
Crystal orientation
Damage threshold
Laser damage accumulation

ABSTRACT

C-, M -, A- and R-plane sapphire plates have been irradiated by a femtosecond laser with different laser parameters. The influences of crystal orientations on irradiation damage of single- and multiple-pulse have been investigated. The experimental results illustrate that the damage morphology, damage threshold, material removal rate and accumulation of laser damage depend on the crystal orientation. This dependence is related to the different bonding energies between adjacent atomic layers for different crystal orientations. The theoretical analysis indicates that bonding energy between adjacent atomic layers of C-, M -, A- and R-plane sapphire plates increases in the order of C-plane < M-plane < A-plane < R-plane. The experimental damage threshold of different crystal planes increases in the order of C-plane < M-plane < A-plane < R-plane and material removal rate decreases in the order of C-plane > M-plane > A-plane > R-plane. The analytical result is in agreement with the experimental result. The experiment results also present that the damage accumulation of M-plane sapphire plates is the largest. Therefore, M-plane is more easily to form cracks under multiple pulse irradiation.

1. Introduction

Sapphire is widely used in aerospace industry, chemical technology, lighting and many other fields due to its excellent physical and chemical properties, which can withstand erosion, irradiation, high temperature, pressure and mechanical loads [1]. Sapphire is an anisotropic brittle crystal with different crystal planes, and the commonly used crystal planes are C-, M -, A- and R-planes. The physical properties of these sapphire plates are different [2,3]. Therefore, sapphire plates with different crystal planes have different industrial applications. For example, C-plane sapphire plates are usually employed as the substrate for light emitting diode (LED) [4]. M-plane sapphire plates have important applications in the growth of non-polar or semi-polar gallium nitride epitaxial films [5]. A-plane sapphire plates are often used as optical window material [6], and R-plane sapphire plates are mainly used in microelectronics products requiring uniform dielectric constant and high insulation properties [7]. However, single-crystal sapphire is difficult to process with mechanical and chemical methods owing to its high hardness (Mohr's hardness of 9, second only to diamond) and chemical inertness. Femtosecond (fs) laser processing has proved to be an effective method to process sapphire because of its high peak power,

small heat-affected zone and high structural accuracy [8]. Machining of sapphire with fs lasers has been studied by many researches. Vilar et al. [9] studied the morphological and structural modifications of sapphire surface processed by fs laser. Chang et al. [10] introduced an effective and direct method in fabricating order-based surface structures of sapphire by fs laser, which can provide a potential process for light extraction and micro-optical applications. Kim et al. [11] reported the formation of polarization-dependent self-ordered nanogratings with a period of about 250 nm on the surface of sapphire by 800 nm fs-laser irradiation. Eberle et al. [12] calculated the ablation threshold of sapphire under different pulse numbers, and found that the ablation threshold of sapphire decreased with increasing pulse number, which is consistent with the cumulative model proposed by Ashkenasi et al. [13,14]. Qi et al. [15] studied fs ablation of C-, A- and R-plane sapphire plates by single and multiple laser pulses irradiation. For single pulse irradiation, two ablation phases were observed and the corresponding threshold fluences of different planes of sapphire plates were calculated. For multiple pulses irradiation, they found that the ablation threshold decreased inversely to the number of laser pulses due to the accumulation effect. Their experimental results revealed that the ablation threshold of sapphire depended on the crystal orientations, in the

* Corresponding author.

E-mail address: qlwen@hqu.edu.cn (Q. Wen).

order of C-plane < A-plane < R-plane. However, the influences of crystal orientations on material removal rate and damage accumulation are lacking, and material removal mechanism of sapphire under fs laser irradiation needs further investigation.

We reported a study of fs laser ablation of C-, M-, A- and R-plane sapphire plates. The Miller indices (hkl) of sapphire plates with different crystal planes were characterized by X-ray diffraction (XRD). The damage morphologies and dimensions of the ablation craters produced by different pulse energies and pulse numbers were evaluated with scanning electron microscopy (SEM) and confocal laser scanning microscope (CLSM). The damage thresholds of C-, M-, A- and R-plane sapphire plates for single and multi-pulse ablations were determined. The impacts of crystal orientations on the damage morphology, crater dimension, damage threshold, material removal rate, and laser damage accumulation were investigated. Furthermore, the material removal mechanism of fs laser ablation of sapphire was analyzed according to the ablation volume of different crystal planes under the same laser condition and the bonding energy between adjacent atomic layers of different crystal planes.

2. Experimental

A commercially available amplified Ti: sapphire laser system (Spitfire, Spectra-Physics) with a center wavelength of 800 nm, a pulse duration of 160 fs, and a repetition rate of 1 kHz was used for the ablation experiments. The incident laser pulse energy E_p goes up to 1 mJ/pulse, which can be calculated from the average output power. The experimental setup is shown in Fig. 1. P-polarized fundamental fs laser (TEM₀₀ mode) emitted from the laser device passes through a half-wave plate, a thin film polarizer, a shutter and a mirror, then is focused perpendicularly to the front surface of specimen via an objective lens (Motic, 2 ×, NA = 0.055). Finally, micro-sized craters are generated on the specimen surface with appropriate laser processing parameters. The black dot array in the dotted box at the lower right of Fig. 1 represents the ablation craters created by fs laser pulses. In the experiment, the laser fluence applied on specimen surface is controlled by a half-wave plate and a thin film polarizer. Moreover, a shutter is used to control the number of laser pulses N applied on the specimen surface.

The specimens are C-, M-, A- and R-plane sapphire plates with dimensions of 10 × 10 × 0.5 mm (length × width × height), which were cut from single-crystalline sapphire, as seen in Fig. 2a. The sapphire plates were polished on both sides with surface roughness smaller

than 0.5 nm. Fig. 2b presents XRD spectra of different crystal planes of sapphire. In Fig. 2b, the lattice plane (006) belongs to C-plane sapphire plate; the lattice plane (300) belongs to M-plane sapphire plate; the lattice planes (110) and (220) belong to A-plane sapphire plate; the lattice planes (012), (024) and (036) belong to R-plane sapphire plate. The diameter of the laser spot (the diameter at $1/e^2$) applied on specimen surface is about 40 μm, which was measured by a charge coupled device (CCD) camera. The specimen was mounted on a three-dimensional (3D) work stage, which was moved by a computer-controlled driving device. All experiments were carried out in ambient air and room temperature. In order to observe the fs laser ablation process of sapphire in real time, LED was used to illuminate the specimen and a CCD camera was used to take pictures of the specimen. SEM and CLSM were used to measure the damage morphologies and dimensions of the ablation craters.

3. Results and discussion

3.1. Influences of laser parameters and crystal orientations on damage features

3.1.1. Single-pulse damage features

Firstly, we studied the evolution of fluence-dependent damage morphologies of sapphire plates for single pulse irradiation. Fig. 3 shows the SEM images of the ablation craters on C-plane sapphire surface created by a single pulse with increased pulse energies. The pulse energy applied onto the sapphire plate is increased from 100 μJ to 340 μJ with a step of 20 μJ. As seen in Fig. 3, the crater morphology is significantly influenced by the laser pulse energy. As the pulse energy $E_p \leq 300 \mu\text{J}$, micro/nano-sized particles are observed within the irradiated region, and the morphology of the ablation craters are irregular. As the pulse energy increases to 320 μJ, the particles within the irradiated region are melted and the etched areas become smooth with no visible features. At pulse energy of 340 μJ, the ablation crater is well defined and crater shape matches well with the laser energy profile (a spatial Gaussian distribution) [10], as seen in Fig. 3f. In addition, as can be seen from Fig. 3 the ablation craters are very shallow, which suggests that the single-pulse ablation only removes the surface material.

3.1.2. Multiple-pulse damage features

We also characterized the morphologies and dimensions of ablation craters on sapphire plates irradiated by multiple laser pulses with

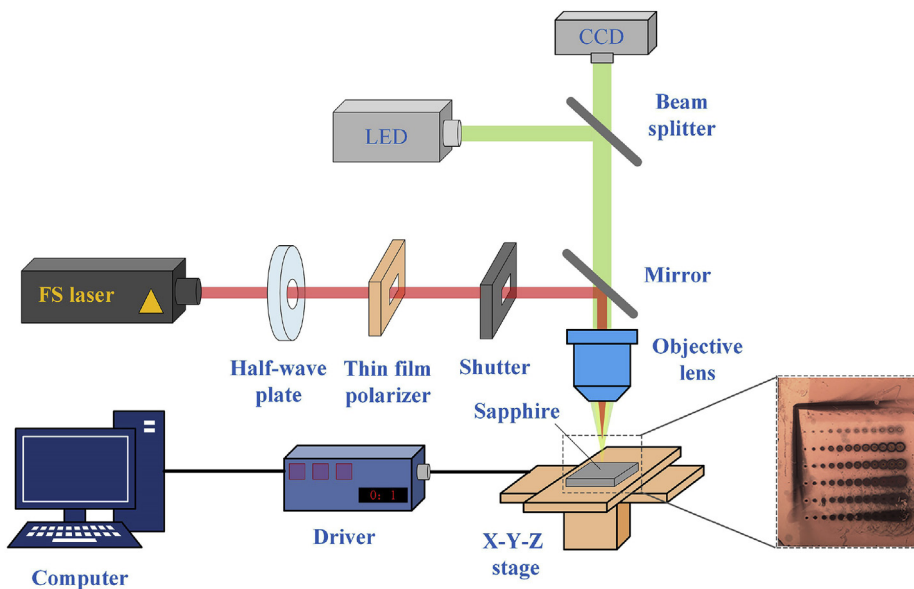


Fig. 1. A schematic diagram of fs laser processing system.

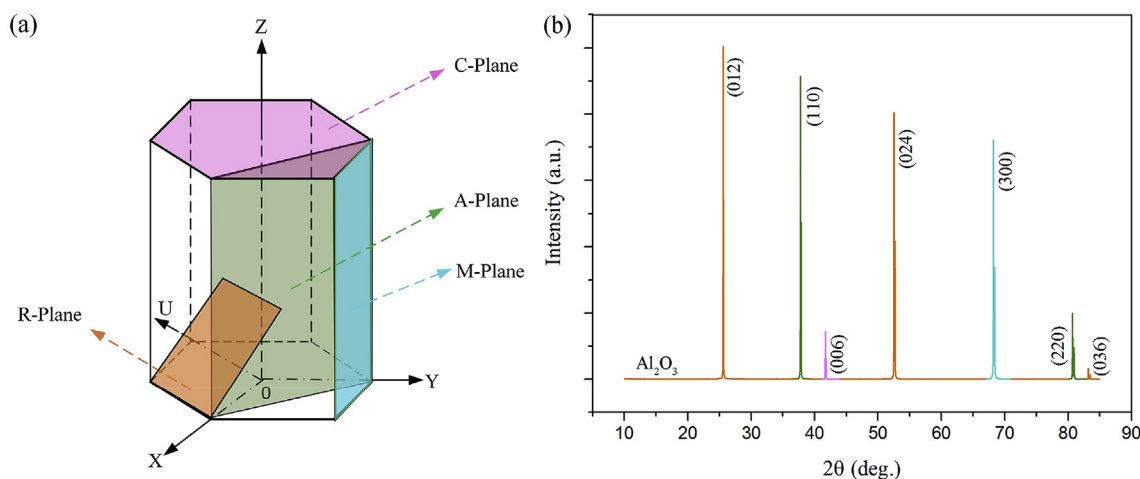


Fig. 2. (a) Crystal structure of sapphire; (b) XRD spectra of different planes of sapphire plates.

different pulse energies. Fig. 4a and b shows the surface morphology of the ablation craters produced by 10 laser pulses at 120 µJ and 140 µJ, respectively. As the pulse energy is 120 µJ, periodic ripples emerge within the ablation crater (Fig. 4a), and the ripple direction is perpendicular to the incident optical electric field. The average ripple period is about 742 nm, which is close to the laser irradiation wavelength (800 nm). The ripple patterns formation can be attributed to constructive interference of the incident laser beam with the scattered surface waves [16,17]. As the pulse energy increases to 140 µJ, the ripple patterns disappear (Fig. 4b). This indicates that the ripple formation is closely related to the pulse energy. Fig. 4a and c shows the SEM images of the ablation craters produced by 10 and 100 laser pulses, respectively, while keeping the laser pulse energy constant at 120 µJ. From Fig. 4a and c, it can be clearly seen that the crater morphology, crater dimension and the ripple formation are greatly influenced by pulse number.

Fig. 5a and b shows the 3D morphology of the ablation craters on C-plane sapphire plate generated by 20 and 100 laser pulses, respectively, while keeping the pulse energy constant at 150 µJ. Under laser irradiation of 20 pulses, the shape of the ablation crater is conical (Fig. 5a), which is attributed to the Gauss distribution of laser energy in the irradiated region. The maximum depth and volume of the ablation crater are about 3.44 µm and 614 µm³, respectively. As pulse number increases to 100, the shape of the ablation crater becomes cylindrical, as shown in Fig. 5b. The average depth of the crater reaches 10.6 µm, and the volume of the ablation crater is about 6207 µm³.

To examine the influences of pulse energy and pulse number on the

depth and volume of the ablation craters, fs laser ablation of sapphire was performed with varied pulse energies and pulse numbers. Fig. 6a shows the volume and average depth of the ablation craters obtained from CLSM-measurements as a function of laser pulse energy under irradiation of 20 laser pulses. As can be seen in Fig. 6a, the average depth of the ablation crater first increases linearly with the laser pulse energy and is saturated after about 110 µJ energy. The ablation volume increases almost linearly with laser pulse energy. Fig. 6b displays the volume and average depth of the ablation crater as a function of pulse number at a fixed pulse energy of 60 µJ. It is seen that the crater volume and average crater depth first increase with pulse number, and eventually reach a saturation value. This is because, as the laser pulse energy and pulse number increase, the ablation crater becomes deeper. At the same time, debris, truncation and scattering occur during the laser propagation, which makes the laser beam unable to penetrate deeper, and the ablation depth gradually becomes saturated [18,19].

3.1.3. Crystal orientation influence on the damage features

We further studied the impact of the crystal orientations of sapphire on the morphologies and sizes of ablation craters produced by the same laser condition. Fig. 7 shows the SEM images of the ablation craters on different planes of sapphire produced by a single pulse at 340 µJ. We noticed that the crater morphologies are closely related to the crystal orientations of sapphire. As seen in Fig. 7, the ablation crater on C-plane sapphire has well defined boundary whereas the boundaries of the ablation craters on, M-, A- and R-plane sapphire plates are shallow. The difference in damage morphology of different crystal

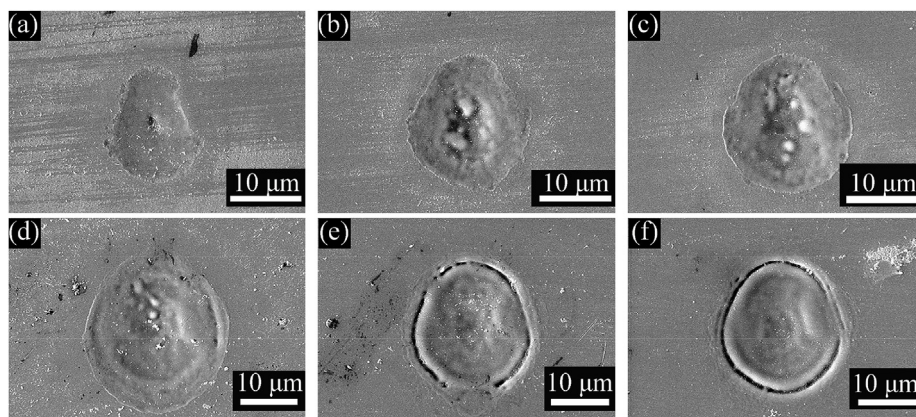


Fig. 3. SEM images of ablation craters on C-plane sapphire plate produced by a single laser pulse with varied pulse energies. (a) 100 µJ; (b) 120 µJ; (c) 140 µJ; (d) 300 µJ; (e) 320 µJ; (f) 340 µJ.

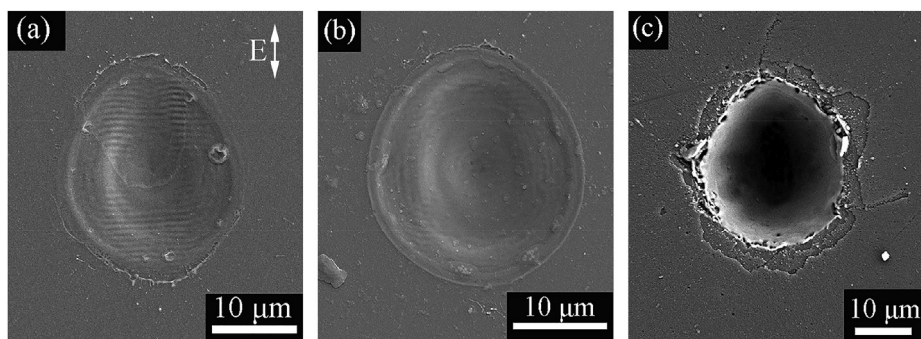


Fig. 4. SEM images of ablation craters on A-plane sapphire plate generated by different pulse energies and pulse numbers. (a) $N = 10$, $E_p = 120 \mu\text{J}$; (b) $N = 10$, $E_p = 140 \mu\text{J}$; (c) $N = 100$, $E_p = 120 \mu\text{J}$. The direction of light polarization is marked by the arrow in (a).

planes is mainly attributed to the different atomic arrangement for different crystal planes. Fig. 8 displays the crater diameter D obtained from SEM-measurements as a function of the laser pulse energy E_p . We can see that the crater diameters increase with increasing laser pulse energy.

Fig. 9 and Fig. 10 show the SEM images of the ablation craters on C-, M-, A- and R-plane sapphire plates generated by 20 and 100 laser pulses, respectively, while keeping the pulse energy constant at 150 μJ. Compared with the surface morphology of ablation craters on sapphire plates under irradiation with 20 pulses, the surface quality becomes poorer under irradiation of 100 pulses, and obvious recast layers are observed at the surrounding area of ablation craters. What's more, cracks are observed inside and outside the crater on M-plane sapphire surface. The crystal orientations of sapphire not only affect the morphology of ablation craters, but also affect the size of ablation craters. Under 20 pulses and 150 μJ energy, the volume and average depth of ablation craters on C-, M-, A- and R-plane sapphire plates are 800, 667, 575, 518 μm³ and 1.68, 1.65, 1.53, 1.42 μm, respectively. As pulse number is increased to 100, the crater volume and average crater depth on C-, M-, A- and R-plane sapphire plates increase to 7220, 5737, 5296, 4788 μm³ and 10.6, 10.0, 9.21, 8.39 μm, respectively. It is found that the volume and depth of the ablation craters produced by the same irradiation condition decrease in the same order of C-plane > M-plane > A-plane > R-plane. This indicates that the material removal rate of C-plane is the highest, followed by M-plane, A-plane and R-plane. The crystal orientation dependent material removal rate might be caused by the different lattice structures of C-, M-, A- and R-plane sapphire plates.

3.2. Material removal mechanism of sapphire by fs laser ablation

The processing parameters of fs laser and the material properties

both have significant influence on the material removal rate [20,21]. Under the same laser processing parameters, the material removal rate of fs laser ablation of sapphire mainly depends on the lattice structure of sapphire with different orientations. Fig. 11 depicts the arrangement of Al³⁺ ion and O²⁻ hollow of adjacent atomic layers of sapphire with different crystal planes [22]. As it can be seen from Fig. 11, the crystal lattice of sapphire (α -Al₂O₃) is formed by Al³⁺ and O²⁻ ions. Bonding in α -Al₂O₃ is mainly ionic, so the largest contribution to the lattice bond energy is the forces of electrostatic interactions [1]. In sapphire crystal, the electrostatic energy per pairs of ions considered as point charges z_1e and z_2e at a distance r apart is given by $u = Az_1z_2e^2/r$, where A is a numerical quantity, of the order of unity, termed the *Madelung constant* [24]. It is apparent that a larger distance r results in a smaller electrostatic energy. Accordingly, we deduce that the lattice bond energy of adjacent atomic layers which belong to different crystal orientations is inversely proportional to the interplanar spacing d of different crystal planes.

The distance between adjacent atomic layers of C-, M-, A- and R-plane sapphire plates can be obtained from the interplanar spacing d for planes (006), (300), (220) and (036), respectively. For hexagonal crystal system, the interplanar spacing d for the plane (hkl) is given by Ref. [23]:

$$d_{hkl} = \frac{1}{\sqrt{\frac{4(h^2 + k^2 + hk)}{3a^2} + \frac{l^2}{c^2}}} \quad (1)$$

here, the lattice constants of sapphire are $a = 4.758 \text{ \AA}$ and $c = 12.992 \text{ \AA}$ at 300 K. The calculated d values of C-, M-, A- and R-plane sapphire plates are 2.165, 1.374, 1.190, 1.160 Å, respectively. This indicates that the interplanar spacing d between adjacent atomic layers of different crystal planes decreases in the order of C-plane > M-plane > A-plane > R-plane. Therefore, the bonding energy for different crystal planes of sapphire increases in the order of C-plane < M-

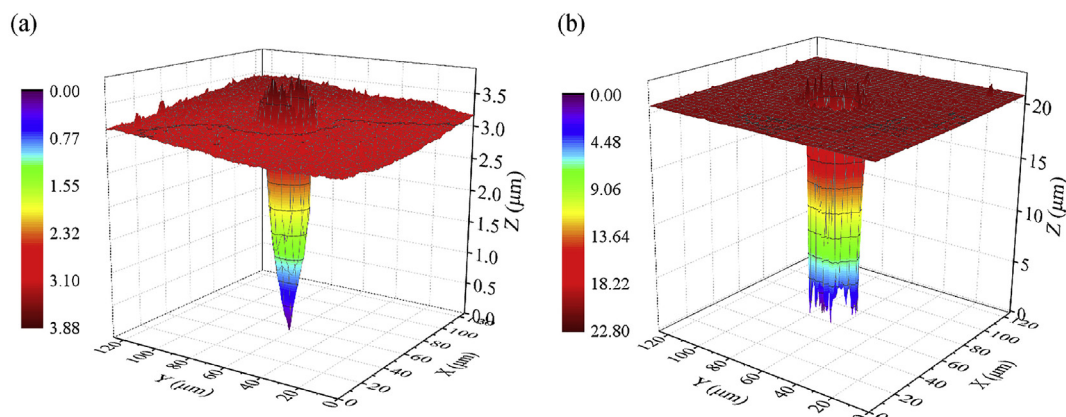


Fig. 5. CLSM image of the ablation craters on C-plane sapphire plate generated by (a) $N = 20$ and (b) $N = 100$ laser pulses at a fixed pulse energy of 150 μJ .

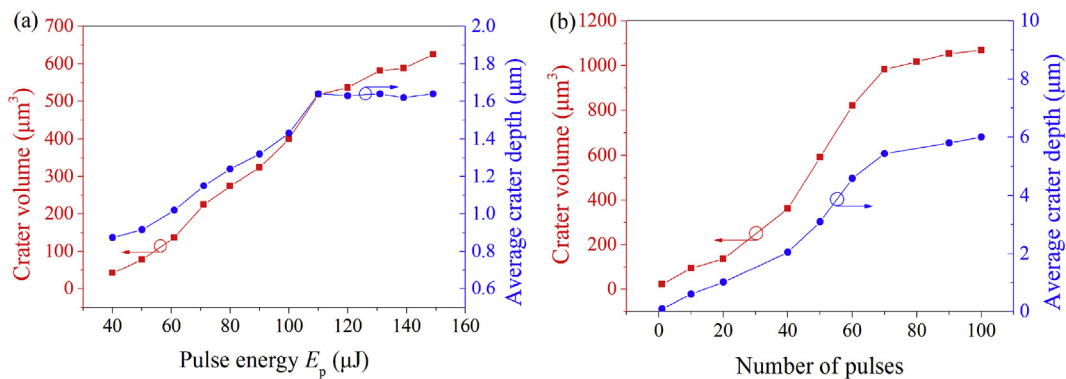


Fig. 6. Volume and average depth of ablation craters on C-plane sapphire vs. (a) pulse energy under irradiation of 20 laser pulses and (b) pulse number under irradiation of 60 μJ energy.

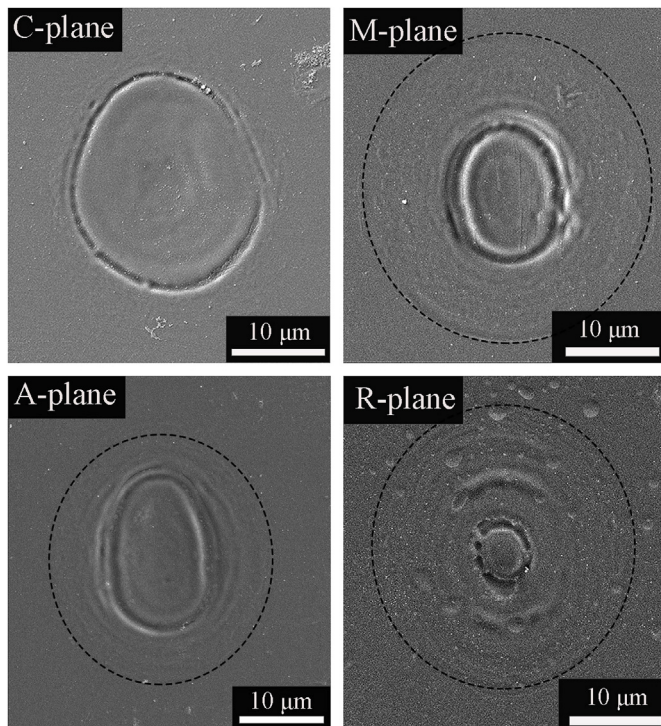


Fig. 7. SEM images of single-pulse fs laser ablation of C-, M-, A- and R-plane sapphire plates at a fixed pulse energy of 340 μJ . The dotted circle represents the crater boundary.

plane < A-plane < R-plane. The smaller the bonding energy, the more easily the material to remove, thus, the material removal rate of sapphire with different orientations decreases in the order of C-plane > M-plane > A-plane > R-plane. This result is in accordance with the descending order of the crater volume obtained from experiment for different planes of sapphire. From the theoretical and experimental results of material removal rate of sapphire with different crystal orientations, we deduce that the material removal mechanism of fs laser ablation is in agreement with that proposed by Kim et al. [25], who believed that materials are removed layer by layer through cracking or exfoliation. However, the interaction between fs laser and materials involves many complex processes, such as coulomb explosion [26], tunneling ionization [27], avalanche ionization [28], so the material removal mechanism of fs laser processing sapphire still needs to be further studied.

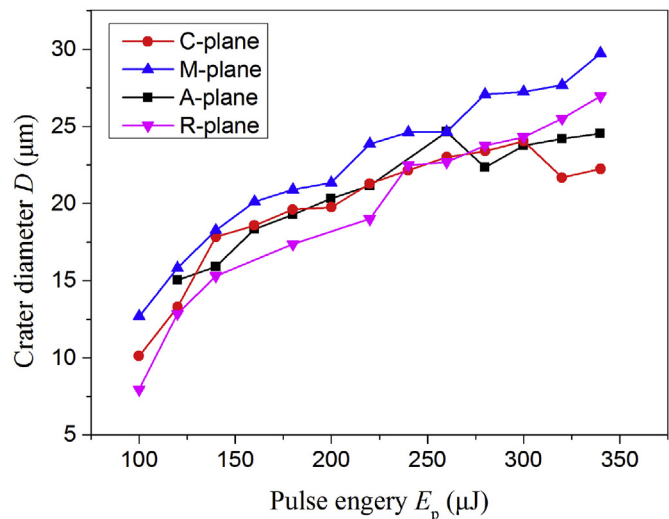


Fig. 8. Crater diameters as a function of laser pulse energy for single-pulse ablation of C-, M-, A- and R-plane sapphire plates.

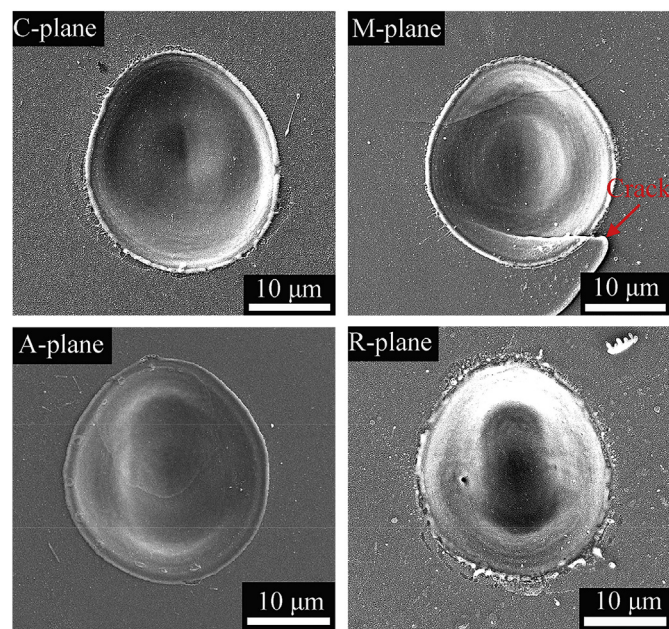


Fig. 9. Morphology of ablation craters on C-, M-, A- and R-plane of sapphire plates generated by 20 pulses and 150 μJ energy.

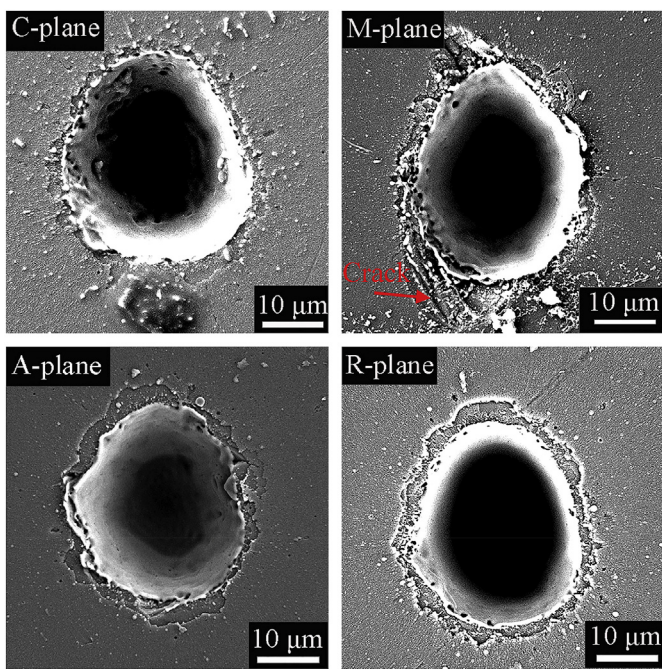


Fig. 10. Morphology of ablation craters on C-, M -, A- and R-plane of sapphire plates generated by 100 pulses and 150 μJ energy.

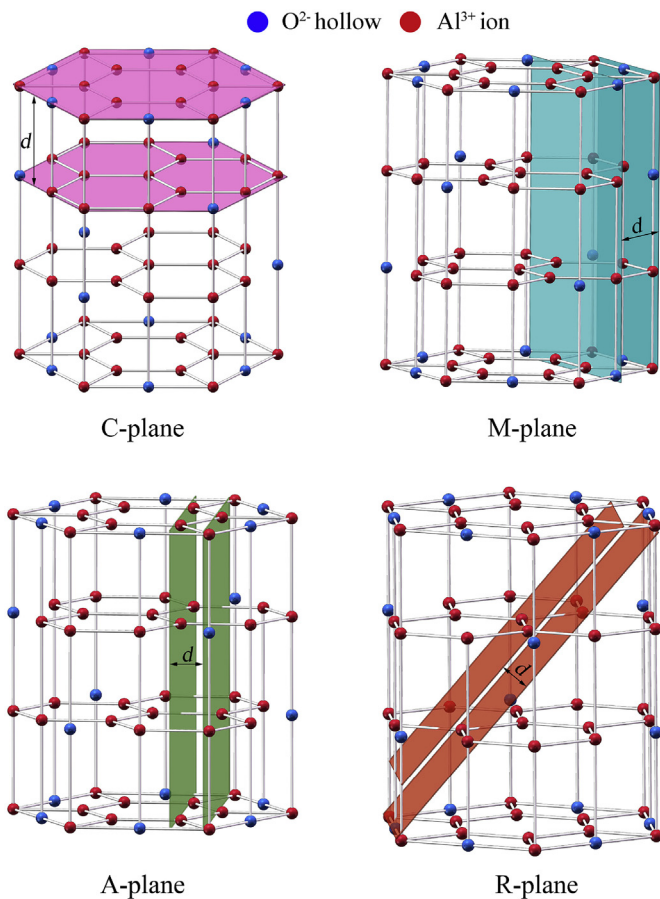


Fig. 11. Crystal models for different orientations of sapphire.

3.3. Damage threshold and accumulation of sapphire with different orientations

In the case of a Gaussian spatial beam profile with a $1/e^2$ -beam radius ω_0 , the maximum laser fluence ϕ_0 applied on the front surface of specimen depends linearly on the incident laser pulse energy E_p [29]:

$$\phi_0 = \frac{2E_p}{\pi\omega_0^2} \quad (2)$$

where ω_0 is 20 μm in the experiment. According to Refs. [30,31], the squared crater diameters D^2 and the maximum laser fluence ϕ_0 applied on the specimen surface satisfies the following equation:

$$D^2 = 2\omega_0^2 \ln\left(\frac{\phi_0}{\phi_{th}}\right) \quad (3)$$

Here ϕ_{th} represents the damage threshold fluence, which is the maximum laser fluence when $D = 0$. From Eq. (3), we can see that the squared diameters D^2 has a linear relationship with $\ln(\phi_0)$. The waist radius ω_0 and the damage threshold fluence ϕ_{th} can be obtained from linear least squares fit.

Fig. 12a and b shows the linear fitting results of D^2 versus $\ln(E_p)$ under single laser pulse and 20 laser pulses irradiation, respectively. The value of ω_0 can be calculated from the slope of the straight line in Fig. 12. In the case of 20 pulses irradiation, the calculated values of ω_0 on C-, M -, A- and R-plane sapphire are 14.8, 14.9, 17.3 and 16.2 μm , respectively, which is close to the ω_0 measured by the CCD camera (20 μm). The difference in the calculated values of ω_0 may be due to measurement errors of crater diameters. The threshold fluence ϕ_{th} can be estimated by extrapolating the linear fit to $D^2 = 0$ in the plot, and the single and multiple pulse threshold fluences of C-, M -, A- and R-plane sapphire plates are shown in Table 1. It is seen that the single pulse damage threshold of C-plane sapphire is $\sim 8.74 \text{ J/cm}^2$, which is very close to the result ($8.4 \pm 0.6 \text{ J/cm}^2$) reported by Christensen et al. [32] under similar laser condition. It is found that, under the same pulse number, the threshold fluence of sapphire with different orientations increases in the order of C-plane < M-plane < A-plane < R-plane, which is consistent with the result reported by Qi et al. [15]. This result indicates that the C-plane sapphire material is more easily to remove than other planes, whereas R-plane sapphire material is the most difficult to remove.

Fig. 13a illustrates the ablation threshold fluence of C-plane sapphire as a function of pulse number. It is seen that the ablation threshold of C-plane sapphire under single pulse irradiation is the largest, and the ablation threshold of sapphire decreases as the pulse number increases, and finally tends to be stable. This result is consistent with a previous report in Ref. [33]. The decrease of the ablation threshold with multi-pulse irradiation is ascribed to the accumulation of laser-induced structural changes of the material and/or deformation of the surface [34].

The effect of cumulative laser action on sapphire surfaces can be described by the accumulation model proposed by Jee et al. [34]. The accumulation of laser damage can be summarized by the following cumulative equation for laser damage:

$$\phi_{th}(N) = \phi_{th}(1) \times N^{s-1}, \quad (4)$$

where $\phi_{th}(N)$ is the multi-pulse damage threshold, $\phi_{th}(1)$ is the single-pulse damage threshold, and s is the accumulation parameter which characterizes the degree of accumulation of laser damage. From Eq. (4), we can see that the smaller the value of s , the stronger the damage accumulation. The value of s is usually less than 1. There is no damage accumulation for $s = 1$. Equation (4) can also be written as follows:

$$\log(N \times \phi_{th}(N)) = \log(\phi_{th}(1)) + s \log(N). \quad (5)$$

From Eq. (5), it is seen that $\log(N \times \phi_{th}(N))$ has a linear relationship with $\log(N)$, as depicted in Fig. 13b. The fitting lines in Fig. 13b

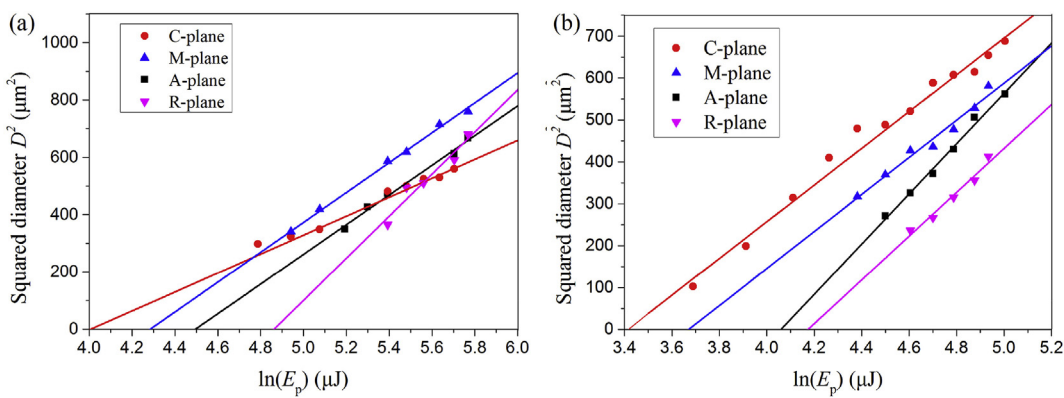


Fig. 12. Squared crater diameters D^2 vs. the logarithm of the applied laser pulse energy $\ln(E_p)$ under irradiation of (a) single pulse and (b) 20 laser pulses.

Table 1
Threshold fluences of sapphire under single- and multi-pulse ablations.

Pulse number N	Threshold fluence ϕ_{th} (J/cm^2)			
	C-plane	M-plane	A-plane	R-plane
1	8.74	11.55	14.26	20.59
10	5.71	6.76	10.56	11.01
20	4.83	6.25	9.22	10.33
100	1.99	2.3	5.9	8.03

represent the damage accumulation curves, and s is the slope of the accumulation curve. We have examined the slope of the accumulation curve for different crystal orientations. The curves have slopes of $s = 0.691$ for C-plane, $s = 0.666$ for M-plane, $s = 0.813$ for A-plane, and $s = 0.794$ for R-plane. Therefore, the damage accumulation of M-plane is stronger than that of other planes. According to Ref. [35], the fracture toughness of C-plane is the largest ($6.043 \text{ MPa m}^{1/2}$), which means C-plane sapphire has the strongest ability to prevent crack formation and propagation. The fracture toughness of M-, A- and R-planes are almost the same, which are 2.509 , 2.509 and $2.152 \text{ MPa m}^{1/2}$, respectively. The experimental results showed that the laser damage accumulation of M-plane is stronger than that of other planes, which indicates the thermal stress on M-plane is the greatest [34]. Therefore, M-plane is more easily to form cracks than other planes under multi-pulse irradiation.

4. Conclusions

We have demonstrated fs laser ablation of C-, M-, A- and R-plane sapphire with different laser parameters. Our results demonstrate that the damage features are strongly affected by the laser parameters and

crystal orientations. The average depth and volume of ablation craters on sapphire plate increase with the increase of pulse energy and pulse number, and finally tend to be a saturation value. For sapphire with different orientations, under the same irradiation condition, the ablation volume increases in the order of R-plane < A-plane < M-plane < C-plane, which indicates the material removal rate of C-plane sapphire is the highest, while that of R-plane is the lowest. The dependence of material removal rate on the crystal orientations is related to the different bonding energies between adjacent atomic layers of different orientations. The theoretical analysis indicates that the bonding energy between adjacent atomic layers of sapphire with different orientations increases in the order of C-plane < M-plane < A-plane < R-plane. According to the experimental results and theoretical analysis, we deduce that the material removal of sapphire by fs laser ablation is peeled atomic layer by atomic layer. The damage threshold and accumulation parameter of different planes of sapphire were also determined. The results show that the damage threshold of sapphire with a fixed orientation decreases with increasing pulse number. For a fixed pulse number, the damage threshold of sapphire with different orientations increases in the order of C-plane < M-plane < A-plane < R-plane. The accumulation of laser damage of M-plane is larger than that of other planes, which means the thermal stress on M-plane is the largest. Therefore, M-plane is more easily to form cracks.

Funding

This work was supported by the National Natural Science Foundation of China (Grant No. 51805176), Youth Natural Science Fund Key Project of Fujian province (Grant No. JZ160412), and Promotion Program for Young and Middle-aged Teacher in Science and Technology Research of Huaqiao University (Grant No. ZQN-PY601).

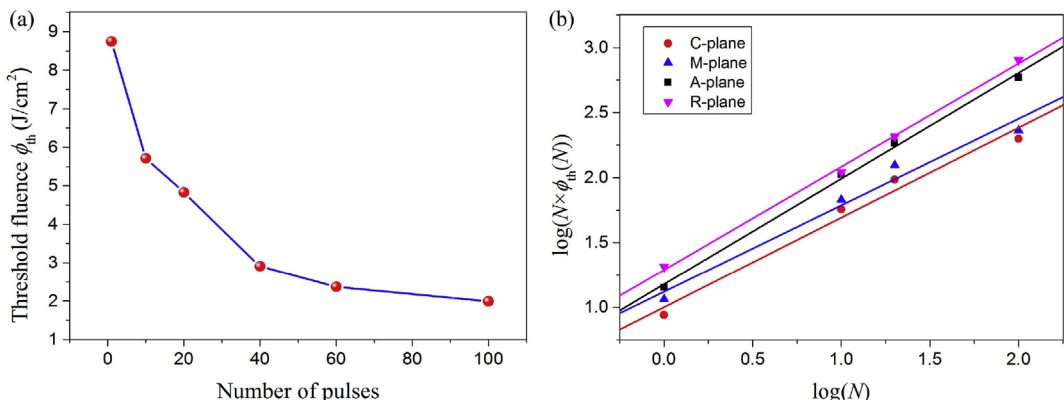


Fig. 13. (a) Threshold fluence of C-plane sapphire vs. pulse number; (b) Threshold fluence $\log(N \times \phi_{th}(N))$ as a function of $\log(N)$ for C-, M-, A- and R-plane sapphire plates.

References

- [1] E.R. Dobrovinskaya, L.A. Lytvynov, V. Pishchik, Sapphire: Material, Manufacturing, Applications, 7–8 (2009), pp. 64–65.
- [2] K. Wang, F. Jiang, L. Yan, X. Xu, N. Wang, X. Zha, X. Lu, Q. Wen, Study on mechanism of crack propagation of sapphire single crystals of four different orientations under impact load and static load, Ceram. Int. 45 (2019) 7359–7375.
- [3] A. Montagne, S. Pathak, X. Maeder, J. Michler, Plasticity and fracture of sapphire at room temperature: load-controlled microcompression of four different orientations, Ceram. Int. 40 (2014) 2083–2090.
- [4] S. Zhou, S. Yuan, Y. Liu, L.J. Guo, S. Liu, H. Ding, Highly efficient and reliable high power LEDs with patterned sapphire wafer and strip-shaped distributed current blocking layer, Appl. Surf. Sci. 355 (2015) 1013–1019.
- [5] Q. Luo, J. Lu, X. Xu, F. Jiang, Removal mechanism of sapphire wafers (0001, 1120 and 1010) in mechanical planarization machining, Ceram. Int. 43 (2017) 16178–16184.
- [6] G. Wang, H. Zuo, H. Zhang, Q. Wu, M. Zhang, X. He, Z. Hu, L. Zhu, Preparation, quality characterization, service performance evaluation and its modification of sapphire crystal for optical window and dome application, Mater. Des. 31 (2010) 706–711.
- [7] W. Wang, W. Yang, H. Wang, Y. Zhu, M. Yang, J. Gao, G. Li, A comparative study on the properties of c-plane and a-plane GaN epitaxial films grown on sapphire wafers by pulsed laser deposition, Vacuum 128 (2016) 158–165.
- [8] K.C. Phillips, H.H. Gandhi, E. Mazur, S.K. Sundaram, Ultrafast laser processing of materials: a review, Adv. Opt. Photon 7 (2015) 684.
- [9] R. Vilar, S.P. Sharma, A. Almeida, L.T. Cangueiro, V. Oliveira, Surface morphology and phase transformations of femtosecond laser-processed sapphire, Appl. Surf. Sci. 288 (2014) 313–323.
- [10] C. Chang, C. Chen, T. Chang, C. Ting, C. Wang, C. Chou, Sapphire surface patterning using femtosecond laser micromachining, Appl. Phys. Mater. Sci. Process 109 (2012) 441–448.
- [11] D. Kim, W. Jang, T. Kim, A. Moon, K. Lim, M. Lee, I. Sohn, S. Jeong, Nanostructure and microripple formation on the surface of sapphire with femtosecond laser pulses, J. Appl. Phys. 111 (2012) 093518.
- [12] G. Eberle, M. Schmidt, F. Pude, K. Wegener, Laser surface and subsurface modification of sapphire using femtosecond pulses, Appl. Surf. Sci. 378 (2016) 504–512.
- [13] D. Ashkenasi, M. Lorenz, R. Stoian, A. Rosenfeld, Surface damage threshold and structuring of dielectrics using femtosecond laser pulses: the role of incubation, Appl. Surf. Sci. 150 (1999) 101–106.
- [14] D. Ashkenasi, R. Stoian, A. Rosenfeld, Single and multiple ultrashort laser pulse ablation threshold of Al₂O₃ (corundum) at different etch phases, Appl. Surf. Sci. 154 (2000) 40–46.
- [15] L. Qi, K. Nishii, M. Yasui, H. Aoki, Y. Namba, Femtosecond laser ablation of sapphire on different crystallographic facet planes by single and multiple laser pulses irradiation, Opt. Lasers Eng. 48 (2010) 1000–1007.
- [16] J. Bonse, M. Munz, H. Sturm, Structure formation on the surface of indium phosphide irradiated by femtosecond laser pulses, J. Appl. Phys. 97 (2005) 013538.
- [17] R. Goodarzi, F. Hajiesmaeilbaigi, Circular ripple formation on the silicon wafer surface after interaction with linearly polarized femtosecond laser pulses in air and water environments, Opt. Quant. Electron. 50 (2018) 299.
- [18] A. Shamir, A.A. Ishaaya, Large volume ablation of Sapphire with ultra-short laser pulses, Appl. Surf. Sci. 270 (2013) 763–766.
- [19] M.E. Shaheen, J.E. Gagnon, B.J. Fryer, Experimental study on 785 nm femtosecond laser ablation of sapphire in air, Laser Phys. Lett. 12 (2015) 66103.
- [20] K. Yin, C. Wang, J.A. Duan, C. Guo, Femtosecond laser-induced periodic surface structural formation on sapphire with nanolayered gold coating, Appl. Phys. Mater. Sci. Process 122 (2016) 834.
- [21] S. He, J.J. Nivas, K.K. Anoop, A. Vecchione, M. Hu, R. Buzzese, S. Amoruso, Surface structures induced by ultrashort laser pulses: formation mechanisms of ripples and grooves, Appl. Surf. Sci. 353 (2015) 1214–1222.
- [22] J. Cheng, J. Wu, Y.D. Gong, X.L. Wen, Q. Wen, Grinding forces in micro slot-grinding (MSG) of single crystal sapphire, Int. J. Mach. Tool Manuf. 112 (2017) 7–20.
- [23] A.R. Verma, Crystallography for Solid State Physics, Wiley, 1982, pp. 74–75.
- [24] R.C. Evans, An Introduction to Crystal Chemistry, CUP Archive, 1964, pp. 45–47.
- [25] S.H. Kim, I. Sohn, S. Jeong, Ablation characteristics of aluminum oxide and nitride ceramics during femtosecond laser micromachining, Appl. Surf. Sci. 255 (2009) 9717–9720.
- [26] W.G. Roeterdink, L.B.F. Juurlink, O.P.H. Vaughan, J. Dura Diez, M. Bonn, A.W. Kleyn, Coulomb explosion in femtosecond laser ablation of Si(111), Appl. Phys. Lett. 82 (2003) 4190–4192.
- [27] C. Wang, L. Jiang, F. Wang, X. Li, Y.P. Yuan, L.T. Qu, Y.F. Lu, Transient localized electron dynamics simulation during femtosecond laser tunnel ionization of diamond, Phys. Lett. A 376 (2012) 3327–3331.
- [28] S.Z. Xu, T.Q. Jia, H.Y. Sun, C.B. Li, X.X. Li, D.H. Feng, J.R. Qiu, Z.Z. Xu, Mechanisms of femtosecond laser-induced breakdown and damage in MgO, Opt. Commun. 259 (2006) 274–280.
- [29] H. Liu, F. Chen, X. Wang, Q. Yang, H. Bian, J. Si, X. Hou, Influence of liquid environments on femtosecond laser ablation of silicon, Thin Solid Films 518 (2010) 5188–5194.
- [30] P. Zhang, L. Chen, J. Chen, Y. Tu, Material removal effect of microchannel processing by femtosecond laser, Opt. Lasers Eng. 98 (2017) 69–75.
- [31] Z. Zhai, W. Wang, J. Zhao, X. Mei, K. Wang, F. Wang, H. Yang, Influence of surface morphology on processing of C/SiC composites via femtosecond laser, Composites Part A 102 (2017) 117–125.
- [32] M.N. Christensen, J. Byskov-Nielsen, B.H. Christensen, P. Balling, Single-shot ablation of sapphire by ultrashort laser pulses, Appl. Phys. A 101 (2010) 279–282.
- [33] X.C. Wang, G.C. Lim, H.Y. Zheng, F.L. Ng, W. Liu, S.J. Chua, Femtosecond pulse laser ablation of sapphire in ambient air, Appl. Surf. Sci. 228 (2004) 221–226.
- [34] Y. Jee, M.F. Becker, R.M. Walser, Laser-induced damage on single-crystal metal surfaces, J. Opt. Soc. Am. B 5 (1988) 648.
- [35] T. Vodenitcharova, L.C. Zhang, I. Zarudi, Y. Yin, H. Domyo, T. Ho, M. Sato, The effect of anisotropy on the deformation and fracture of sapphire wafers subjected to thermal shocks, J. Mater. Process. Technol. 194 (2007) 52–62.